Nonlinear Dynamics **32:** 187–209, 2003.
© 2003 *Kluwer Academic Publishers. Printed in the Netherlands.*

PC145

Bifurcations of a Thin Plate-Strip Excited Transversally and Axially

J. AWREJCEWICZ
Department of Automatics and Biomechanics, Technical University of Lodz, Stefanowskiego 1/15, PL-90-924 Lodz, Poland

V. A. KRYSKO and G. G. NARKAITIS
Department of Mathematics, Saratov State University, 41005 Saratov, Russia

(Received: 13 June 2002; accepted: 18 March 2003)

Abstract. The complex vibrations and bifurcations of plates modeled as systems with infinite degrees-of-freedom are considered. Both the Bubnov–Galerkin with high-order approximations and finite difference methods with approximation $O(h^4)$ are applied. In addition, the calculation of the Lyapunov exponents of the system is performed, and the results are compared to those derived by Bennetin's method. Some examples of new nonlinear phenomena exhibited by the considered systems are reported.

Keywords: Bifurcation, chaos, plate, Bubnov–Galerkin and finite difference methods.

1. Introduction

The nonlinear dynamics of plates (shells) has been well studied in the literature. First, it should be noted that plates (shells) are members of various engineering structures and their behavior should be completely understood. A complete and exact knowledge of plate (shell) statics or dynamics must contain a full three-dimensional field, which is very often too difficult for a general analysis; hence, the so-called low dimensional models are often applied [1–4]. Second, the mathematical models of plate dynamics within the Kirchhoff–Love or von Kármán hypothesis can serve to verify low-dimensional spatially localized models of extended systems represented by plates or shells. Attempts at building low-dimensional systems capturing the key features of extended systems has a long history. The idea is focused on the projection of the investigated partial differential equation(s) into the most energetic modes obtained either through the Bubnov–Galerkin projection or via proper orthogonal decomposition.

Although parametric vibrations of flexible plates of infinite length are considered in a series of publications, in a majority of them the continuous system is analyzed as a one-degree-of-freedom system. The method of multiple scales is used by Abe et al. [5] to analyze the two-mode response of simply supported laminated plates subjected to harmonic excitation. The multiple-scales technique is applied to analyze subharmonic traveling waves of thin, axisymmetric, and geometrically nonlinear circular plates [6]. Recently Wei Zhang et al. [7] used the Galerkin method (in the present paper, the method is further called Bubnov–Galerkin, since it has been developed by Bubnov) to derive the averaged equations from the von Kármán equation and to analyze both local and global bifurcations of a parametrically and externally excited simply supported rectangular thin plate.

Third, various models governing nonlinear dynamics of plates and shells possess their own history and still require a rigorous mathematical treatment. For example, we briefly mention the von Kármán equation considered in [7]. Finite dimensionality and compactness of attractors for the von Kármán equation are considered by Lasiecka [8], and more generalized questions are also addressed in [9–11].

In spite of some new results devoted to bifurcation and chaos exhibited by thin infinite length plate dynamics, another important problem has to be solved. Note that usually the partial differential equations governing the behavior of continuous systems are transformed to a nonlinear set of ordinary differential equations using the Bubnov–Galerkin procedure without a rigorous motivation and the error estimation. This question is illustrated and discussed in the paper, and in addition the finite difference method is applied which gives 'almost' exact results [12], and hence it serves as a tool for a validity estimation of higher-order Bubnov–Galerkin procedures.

2. Fundamental Relations

Nonlinear vibrations of a rectangular plate subjected to longitudinal sign-changing load are analyzed. It is assumed that one of the plate dimensions is significantly larger than the other one, i.e. $b \gg a$. The behavior of the parts of the plate that lie close to its shorter edges is beyond considerations, and it is assumed that the plate bends to a cylindrical surface along the other dimension. Therefore, it is sufficient to study vibrations of a beam flange (or a plate-strip) of length a and of unit width. Note that the introduced assumptions lead to essential simplifications of the problem, since in the von Kármán equations, only one spatial variable x appears (instead of two). The following equation is analyzed [13]:

$$\frac{h}{\gamma g}\ddot{w} + h\varepsilon\dot{w} = -D\frac{\partial^4 w}{\partial x^4} + \frac{Eh}{2b(1-\nu^2)}\frac{\partial^2 w}{\partial x^2}\left\{\int_0^b \left(\frac{\partial w}{\partial x}\right)^2 \mathrm{d}x\right\} - P_x(t)\frac{\partial^2 w}{\partial x^2} + q(x,t), \tag{2.1}$$

where a is the beam flange (or plate-strip) dimension; h denotes its thickness; $P_x(t)$, $q(x,t)$ are the longitudinal and transverse loads, respectively; E is the elasticity modulus of an isotropic material; $D = Eh^3/(12(1-\nu^2))$ is the cylindrical stiffness; ν is Poisson's coefficient; γ is the specific weight of the plate material; g denotes gravity acceleration.

The following nondimensional (with bars) quantities are introduced:

$$x = \bar{x}b, \quad w = h\bar{w}, \quad P = \frac{Eh^3}{a^2}\bar{P}, \quad q = \frac{Eh^4}{a^4}\bar{q}, \quad t = \frac{a^2}{h}\left(\frac{\gamma}{Eg}\right)^{1/2}\bar{t},$$

$$\varepsilon = \frac{a^2}{h^2}\left(\frac{\gamma}{Eh^2 g}\right)^{1/2}\bar{\varepsilon}, \quad \lambda = \frac{1}{12(1-\nu^2)},$$

and the nondimensional governing equation follows (bars are omitted):

$$\ddot{w} + \varepsilon\dot{w} = -\lambda\frac{\partial^4 w}{\partial x^4} + 6\lambda\left\{\int_0^1 \left(\frac{\partial w}{\partial x}\right)^2 \mathrm{d}x\right\}\frac{\partial^2 w}{\partial x^2}$$

$$- P_x(t)\frac{\partial^2 w}{\partial x^2} + q(x,t), \quad 0 \le x \le 1; \quad t \in (0,\infty). \tag{2.2}$$

Note that in both Equations (2.1) and (2.2) dissipative properties of the system are proportional to its velocity. On the other hand, it is well known that various models of dissipative properties exist.

Both linear and nonlinear friction descriptions can be applied yielding various analytical friction approximations. Recall that during a cyclic load Hooke's law may be replaced by hysteresis behavior indicating energy dissipation per cycle in the unit material volume. It has been experimentally verified that the hysteresis loop does not depend on the rate of deformations (i.e. on a frequency), but only on the deformation amplitude.

Here linear dissipation is considered. It is worth noticing that the introduction of dissipative terms (when a constant transversal load is applied) leads to a solution of a static problem, since for a critical damping value, vibrations are rapidly damped and one obtains a solution of the stationary problem. The described approach was first applied by Fedosev [14]. Note that the dissipative terms can be introduced also for solving large algebraic systems, and the yielded iterational scheme possesses more advantages, in comparison to the classical [11] Newton approach.

In the case of time-dependent loads $\dot{P}_x(t)$, $q(x,t)$, the ε value plays a crucial role during the investigation of vibrations and chaos thresholds. Recall that in the case of a one-degree-of-freedom linear oscillator we have

$$d\ddot{w} + \varepsilon\dot{w} + cw = 0, \tag{2.3}$$

where d is an inertial coefficient, c denotes stiffness, and ε is damping. For $\varepsilon < 2\sqrt{ac}$ the oscillations are damped, and damping plays a negligible influence on frequency of oscillations. For $\varepsilon > 2\sqrt{ac}$ oscillations do not appear ($\varepsilon_{cr} = 2\sqrt{ac}$).

The following boundary conditions are associated with Equation (2.2):

$$w = w''_{xx} = 0 \quad \text{for } x = 0;\ 1, \tag{2.4}$$

$$w = w'_x = 0 \quad \text{for } x = 0;\ 1. \tag{2.5}$$

The initial conditions are:

$$w(x)|_{t=0} = 0.01 \sin \pi x, \quad \dot{w}(x)|_{t=0} = 0, \tag{2.6}$$

$$w(x)|_{t=0} = 0.01(1 - \cos 2\pi x), \quad \dot{w}(x)|_{t=0} = 0, \tag{2.7}$$

A solution to this Cauchy problem is found by using two approaches, i.e., the Bubnov–Galerkin (BG) method and the finite differences (FD) method with approximation of $O(h^4)$. Recall, that the Bubnov–Galerkin method reduces the initial-boundary problem to that of solution to a system of ordinary differential equations.

Assume a solution in the form

$$w(x,t) = \sum_{i=0}^{N} A_i(t) w_i(x), \tag{2.8}$$

where $w_i(x)$ should satisfy one of the given boundary conditions (2.4), (2.5). Applying the Bubnov–Galerkin procedure to Equation (2.2) the following system of ordinary differential equations for $A_i(t)$ is obtained:

$$\sum_{i=0}^{N}(\ddot{A}_i + \varepsilon\dot{A}_i)a_{ik} = -\lambda\sum_{i=0}^{N}A_i b_{ik} + 6\lambda L(A_i(t))\sum_{i=0}^{N}A_i c_{ik} - P_x(t)\sum_{i=0}^{N}A_i c_{ik} + Q_k(t), \tag{2.9}$$

where $k = 0, 1, \ldots$.

In the above, the following notations are used:

$$a_{ik} = \int_0^1 w_i(x)w_k(x)\,dx, \quad b_{ik} = \int_0^1 w_i^{IV}(x)w_k(x)\,dx, \quad c_{ik} = \int_0^1 w_i''(x)w_k(x),$$

$$Q_k = \int_0^1 q(t,x)w_k(x)\,dx, \quad L(A_i(t)) = \int_0^1 \left(\sum_{i=0}^{N}A_i(t)w_i'\right)^2 dx. \tag{2.10}$$

It is easy to reduce these second-order differential equations to first-order ones and then to solve them using, for example, the Runge–Kutta method.

3. Finite Difference Method

To reduce the partial differential equations (2.2) to ordinary differential equations the finite difference method with approximation $O(h^4)$ is applied to the spatial coordinate x. In the grid space

$$G_k = \left\{0 \le x_i \le 1, \quad x_i = ih, \quad h = \frac{1}{N}, \quad i = 1, \ldots, N\right\},$$

the partial derivatives are substituted for the difference approximations

$$\left(\frac{\partial(\cdot)}{\partial x}\right)_i \approx \frac{1}{12h}[(\cdot)_{i-2} - 8(\cdot)_{i-1} + 8(\cdot)_{i+1} - (\cdot)_{i+2}] = \Lambda_x(\cdot) + O(h^4), \tag{3.1}$$

$$\left(\frac{\partial^2(\cdot)}{\partial x^2}\right)_i \approx \frac{1}{h^2}[(\cdot)_{i-2} + 16(\cdot)_{i+1} - 30(\cdot)_i + 16(\cdot)_{i-1} + (\cdot)_{i-2}] = \Lambda_{x^2}(\cdot) + O(h^4), \tag{3.2}$$

$$\left(\frac{\partial^4(\cdot)}{\partial x^4}\right)_i \approx \frac{1}{6h^4}[-(\cdot)_{i+3} + 12(\cdot)_{i+2} - 39(\cdot)_{i+1} + 56(\cdot)_i - 39(\cdot)_{i-1} + 12(\cdot)_i - 2 - (\cdot)_{i-3}]$$
$$= \Lambda_{x^4}(\cdot) + O(h^4), \tag{3.3}$$

and Equation (2.2) is transformed to the following set of equations:

$$\ddot{w}_i + \varepsilon \dot{w}_i = -\lambda \Lambda_{x^4}(w_i) + 6\lambda \left\{ \int_0^1 (\Lambda_x(w_i))^2 \, dx \right\} \Lambda_{x^2}(w_i) - P_x(t) \Lambda_{x^2}(w_i) + q(ih, t). \tag{3.4}$$

Note that the integrations in Equations (3.4) are carried out using Simpson's formula. Applying the approximation we have two series of the out-contour points. The following observations hold for the boundary conditions (2.4), (2.5):

(i) for the balls supported edge $(\cdot)_{-i} = -(\cdot)_i$,
(ii) for the clamped edge $(\cdot)_{-i} = -(\cdot)_i$.

Introducing the change of variables

$$\dot{w}_i = w_i', \tag{3.5}$$

Equation (3.4) is reduced to the following first-order differential equations with respect to the deflections w_i and velocities w_i'

$$\dot{w}_i' + \varepsilon w_i' = -\lambda \Lambda_{x^4}(w_i) + 6\lambda \left\{ \int_0^1 (\Lambda_x(w_i))^2 \, dx \right\} \Lambda_{x^2}(w_i) - P_x(t) \Lambda_{x^2}(w_i) + q(ih, t). \tag{3.6}$$

The obtained ODEs (3.5), (3.6) are solved using the second-order Runge–Kutta method.

As has already been mentioned, two different computational methods are used to solve the earlier formulated problem (the Bubnov–Galerkin method with higher approximations and the finite difference method). Note that the application of the two different approaches is necessary to obtain reliable results. In addition, the finite difference method may serve as a criterion to estimate the accuracy of the lumped system approximation. Note that in many papers, either one or two modes are taken into account, i.e. the problem of continuous system is substituted by that of one or two degrees-of-freedom. Then usually many important conclusions are arrived at in relation to simple lumped systems. However, the question concerning such approximation validity is very rarely discussed. Our methodology is formulated in a completely different manner. We are focused on the initially formulated problem of flexible plate dynamics and we use two computational methods (which practically give exact results) to solve the considered partial differential equation.

4. Application of the Bubnov–Galerkin Method to Equations (2.2), (2.4) and (2.6)

A solution to Equation (2.8) is sought in the form

$$w_i(x) = \sin(2i + 1)\pi x. \tag{4.1}$$

In the case of parametric vibrations $P_x(t) = P_0 \sin(\omega_p t)$ and for the lack of transversal load $q(t, x) = 0$, the system (2.9) is transformed to the following one-degree-of-freedom system:

$$\ddot{A}_0(t) + \varepsilon \dot{A}_0(t) + (\pi^4 \lambda + \pi^2 P_x(t)) A_0(t) + 3\pi^4 \lambda A_0^3(t) = 0. \tag{4.2}$$

The so obtained second-order ordinary differential equation, after the variables change, is reduced to a system of two first-order ordinary differential equations which are then solved using the second-order Runge–Kutta method.

5. Lyapunov Characteristic Exponents

It is well known that the Lyapunov exponents play an important role in the theory of dissipative dynamical systems, since they give a qualitative measure of chaotic behavior. On the other hand, there exists a relationship between the Lyapunov exponents and other measures of chaotic processes like, for example, Kolmogorov's entropy or dynamical dimension. Besides, there is also a connection between Lyapunov exponents and mechanical vibrations of the plate constructions, which will be discussed further.

We briefly recall the well-known algorithm used to compute Lyapunov characteristic exponents. The theory of Lyapunov exponents has been applied by Oseledec [15]. A connection between the Laypunov exponents and Kolmogorov entropy has been considered by Bennetin et al. [16, 17] and rigorously formulated by Peshin [18]. In the literature devoted to the investigation of chaotic vibrations of various dynamical systems, the method proposed by Benettin et al. is widely used [16, 17]. Therefore, we focus on the brief description of the method outlining some drawbacks with respect to its numerical realization.

First, an arbitrary system consisting of n-dimensional vectors is chosen (n denotes the dimension of the phase space). The analyzed system of differential equations together with the associated linearized one is integrated on a certain interval and a new system of vectors x_i is yielded.

The obtained system is normalized using the Gramm–Schmidt algorithm and is taken as a new system of vectors x_i for the next computation step. The logarithms of normalized coefficients are averaged for each of the vectors on a sufficiently large number of such iterations and the limits of the iteration series give a spectrum of Lyapunov exponents. Note that the initial system should be (in the beginning) in a stationary state and the phase point at the end of the interval of each integration step serves as the initial condition for the next interval.

Bennetin et al. [16, 17] have already shown that the choice of the initial system of the vectors may be arbitrary and does not influence the limiting values of the Lyapunov exponents.

In practice, it is recommended that both the linearized system and the nonlinear one are integrated by using one integration method. It means that the computational algorithm is of $n+1$ higher complexity than that applied to the investigated original nonlinear system. In addition, in order to achieve the required accuracy, an orthogonalization procedure should be introduced in each of the Runge–Kutta integration steps. Note that an increase of the interval, where the integration of the linearized system is carried out, yields a decrease of the angle values between the vectors x_i, which finally introduces a rather large error itno the orthonormalization process. This also leads to an extension of the algorithm complexity and computational time. However, for low-dimensional systems one may solve the problem in an analytical way. For instance, for our system (4.2) the associated Jacobian has the form

$$I(A_0, t) = \begin{pmatrix} 0 & 1 \\ -\frac{\pi^2}{12(1-\nu^2)} - 3\frac{\pi^2}{4(1-\nu^2)}A_0(t)^2 + P_x(t) & -\varepsilon \end{pmatrix}. \tag{5.1}$$

Assuming λ_1, λ_2 to be eigenvalues of the Jacobian, one may solve the system of differential equations $\dot{A} = I \times A$ with initial conditions

$$A(0) = \begin{pmatrix} A_0 & (0) \\ \dot{A}_0 & (0) \end{pmatrix}$$

to get

$$A(t) = \begin{pmatrix} \frac{1}{\lambda_1 - \lambda_2}\{(-\lambda_2 A_0(0) + \dot{A}_0))\, e^{\lambda_1 t} - (-\lambda_{11} A_0(0) + \dot{A}_0(0))\, e^{\lambda_2 t}\} \\ \frac{1}{\lambda_1 - \lambda_2}\{\lambda_1(-\lambda_2 A_0(0) + \dot{A}_0))\, e^{\lambda_1 t} - \lambda_2(-\lambda_{11} A_0(0) + \dot{A}_0(0))\, e^{\lambda_2 t}\} \end{pmatrix}. \tag{5.2}$$

Observe that in general λ_1 and λ_2 are complex values and hence the latter formula has different representations for complex and purely real λ. Therefore, the mentioned drawbacks of the Lyapunov exponent computation are avoided here, since instead of numerical integrations, we apply the analytic formula (5.2). This proposed approach essentially decreases the computational time and increases the accuracy of the results. A comparison of the two described methods shows that in practice they are equivalent. Indeed, the difference in results is less than 0.1%.

The analytical form (5.2) also has a physical interpretation. Observe that the length of the vectors exponentially increases (decreases) with respect to the real parts of λ_1 and λ_2.

Therefore, the computation of the Lyapunov exponents can be estimated by direct averaging of the real parts of the Jacobian matrix eigenvalues along the investigated phase curve. The proposed method is more suitable to estimate Lyapunov exponents compared to the classical one, which is only an approximate numerical realization of the original idea. However, the proposed method can be applicable only in the case of rather narrow class of dynamical systems, where the eigenvalues of the Jacobian can be computed analytically.

Observe that in the case of a plate with infinite length (plate-strip) one may obtain

$$\lambda_{1,2} = -\frac{\varepsilon}{2} \pm \sqrt{\left(\frac{\varepsilon}{2}\right)^2 - \frac{\pi^2}{12(1-\nu^2)} - 3\frac{\pi^2}{4(1-\nu^2)} A_0(t)^2 - P_x(t)}. \tag{5.3}$$

Therefore, the spectrum of Lyapunov exponents (χ_1, χ_2) satisfies the following properties: $\chi_1 + \chi_2 = -\varepsilon$ and $\chi_2 < 0$. The following analytical condition serves as chaos occurrence criterion:

$$\chi_1 \geq 0 \Rightarrow \lim_{t\to\infty} \int_0^t \operatorname{Re}\left(\sqrt{\left(\frac{\varepsilon}{2}\right)^2 - \frac{\pi^2}{12(1-\nu^2)} - 3\frac{\pi^2}{4(1-\nu^2)} A_0(t)^2 - P_x(t)}\right) \mathrm{d}t$$

$$\geq \frac{\varepsilon}{2}. \tag{5.4}$$

This approach has many more advantages in comparison to the classical one. A number of additional operations is small and almost the whole computational time is focused on integration of the nonlinear system.

In addition, the speed of convergence is higher than in the classical approach, which may be very important for large computations.

However, although the qualitative behavior of these two methods is similar, quantitative differences are expected. As an example, a comparison of the computations of maximal Lyapunov exponent *versus* excitation amplitude P_x for fixed ω_p is equal to the eigenfrequency of the considered system is shown in Figure 1. The results obtained coincide well with the Fourier analysis (FFT) of these vibrations. In other words, the harmonic vibrations correspond

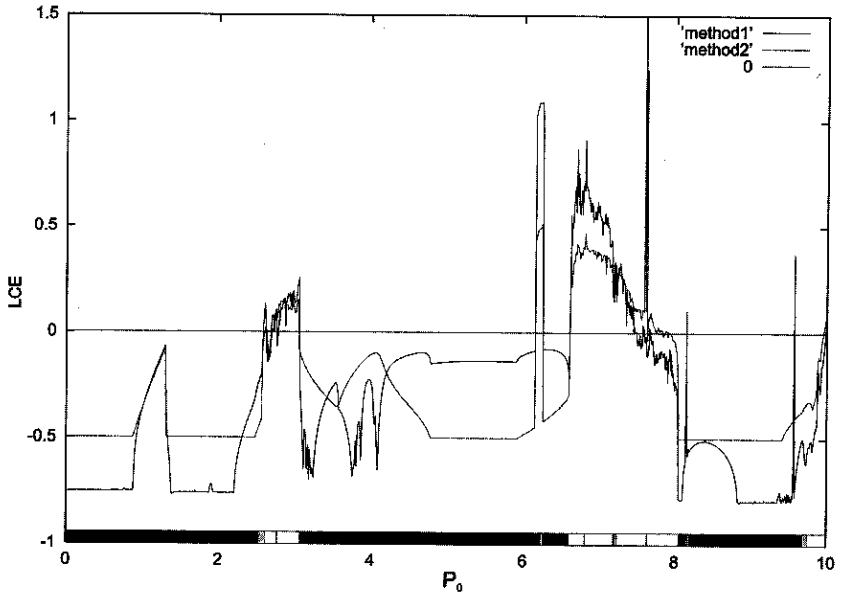

Figure 1. Lyapunov characteristic exponent estimated using the Bennettin [16, 17] method (method 1) and our method (method 2) *versus* P_0.

to negative values of the maximal Lyapunov exponent, chaotic vibrations correspond to its positive value, and in the case of a bifurcation, χ_1 is close to 0.

6. Application of the Bubnov–Galerkin and Finite Difference Methods (Problem 1)

The system of Equations (2.2), (2.4) and (2.6) is solved by using both the Bubnov–Galerkin and finite difference methods. The investigations are focused on a construction of a plate vibration chart in the parameter plane (P_0, ω_p) for each of the boundary conditions $(q(x, t) = 0)$. It has been observed that vibrations are fully defined by the vibrations of the center of the plane $(x = 0.5)$, since other plate points move in a synchronized way. The intervals $0.5\omega_0 < \omega_p < 1.5\omega_0$ are applied while constructing the charts, where ω_0 is the eigenfrequency of the plate for given boundary conditions. The interval of P_0 variation is chosen in such a way that a maximal deflection does not achieve 7 times that of the plate thickness.

For the boundary conditions (2.4) the eigenfrequency $\omega_0 = 3$, and the interval of the construction of the charts is equal to [1.5; 4.5]. Variation in the interval is [0; 50]. The chart corresponding to the applied boundary conditions is reported in Figure 2. Observe that results obtained using either the Bubnov–Galerkin or finite difference methods are identical, which proves their reality (true values).

The following important key numerical values are taken. In the Bubnov–Galerkin the time step $\mathrm{d}t = 0.0078125$ is used. In the finite difference method $n = 16$ ($\mathrm{d}x = 0.0625$). Those parameters are found from Runge's rule and they guarantee convergence of the harmonic vibrations.

Let us now analyze the chart reported in Figure 2. We trace the dynamics by observing the cross-sections along the P_0 axis, which corresponds to the change of external amplitude excitation with its constant frequency. Applying this type of analysis one may separate the

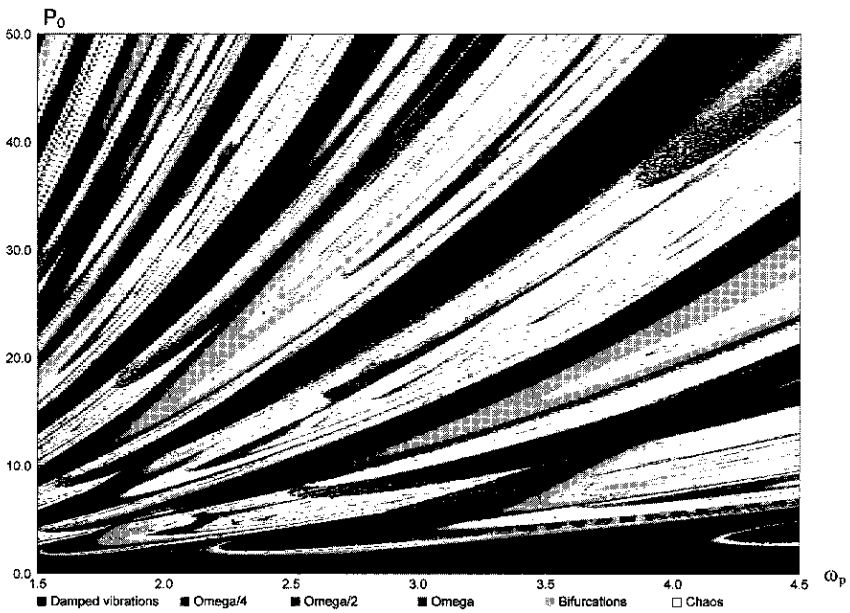

Figure 2. Regular and chaotic dynamics in the plane (P_0, ω_p).

plane into three parts: [1.5; 2.2] – low frequencies; [2.2; 3.8] – average frequencies; [3.8; 4.5] – high frequencies.

For small values of amplitudes of the exciting force the introduced energy to the system is too small to realize the undamped stationary vibrations. The lowest part of the chart corresponds to damped vibrations. The first 'stiff' bifurcation is represented by the top boundary of this part. In other words, a slight increase in the amplitude of external excitation yields a qualitative change of vibrations. A transition from damped to harmonic vibrations takes place. In addition, two different cases may be distinguished after 'stiff' bifurcation: the frequency of vibrations is either equal to the external excitation frequency or it is half as large. This frequency serves as a criterion for partition of the plane into different frequency zones.

For zones of low and high frequencies, vibrations with $\omega_p/2$ appear, whereas for zones of averaged frequencies, vibrations with ω_p occur. The numerical results obtained suggest that the harmonic plate vibrations are possible only for three following frequencies: $\omega_p/4$, $\omega_p/2$, and ω_p.

We briefly follow the scenario of bifurcations for the average frequencies zone. After 'stiff' bifurcation the harmonic vibrations with the frequency ω_p appear. A further increase in P_0 leads to a series of bifurcations and transition to chaotic vibrations. Then, again harmonic vibrations appear, but with the frequency ω_p and the related transition is not associated with a series of bifurcations. A similar scheme of frequency switching is also typical for two other parts of the parameter plane with only one difference: instead of the initial frequency ω_p, now $\omega_p/2$ appears.

In addition, in the investigated chart, the areas with harmonic vibrations with the frequency $\omega_p/4$, and the areas where bifurcations are observed, are separated.

For areas with bifurcations, two special cases are addressed: (i) a transition from harmonic to chaotic vibrations, and (ii) internal areas of zones of harmonic vibrations.

Table 1. Amplitudes of parametric excitation P_0^n, and the Feigenbaum constants C_i for the problem 1 (n denotes bifurcation number).

n	1	2	3	4	5	6	7	8
P_0^n	2.573266	2.603611	2.313630	2.616151	2.616679	2.616790	2.616814	2.618190
C_i		3.028	3.975	4.770	4.759	4.708	4.683	

The singular cases occurring on the borders between frequency zones are investigated separately. Jump-like switching between frequencies is observed, i.e. either a lack of bifurcation series or transition to chaos is detected. The frequency zones discussed are: [2.1; 2.2] and [3.8; 4.2].

For the mentioned frequency intervals, one may observe 'stiff' bifurcation twice. After the first 'stiff' bifurcation, stable harmonic vibrations appear. Next, on the short interval of the vibrations again are damped. Then 'stiff' bifurcation occurs again, and the harmonic vibrations with a different frequency appear.

Following the introduction of the chart, one may also detect self-similarity of its parts, particularly in the part corresponding to small amplitudes of external force. The shapes of areas are repeated in all three zones, and higher frequencies correspond to larger area dimension. As it has been already mentioned, neighboring zones are distinguished through switching of frequency order for harmonic vibrations. Therefore, similar areas have only qualitatively the same vibrations, but they may differ with respect to quantized exponents.

Since, on the same intervals of parameter changes, a route to chaos is associated with a bifurcation series, the problem of comparison with the Feigenbaum scenario is addressed. The first route to chaos in the zone of averaged frequencies is investigated in more detail.

The first eight bifurcations are numerically traced using the Bubnov–Galerkin method. As an example, the data obtained for the eigenfrequency required for the Feigenbaum constant computation are reported in Table 1.

The obtained results coincide very well with the theoretically obtained value

$$C_\infty = \lim_{n\to\infty} \frac{P_x^n - P_x^{n-1}}{P_x^{n+1} - P_x^n} \approx 4.6692\ldots.$$

In Figure 3 the frequency spectrum for $\omega_p = \omega_0 = 0$, $P_0^8 = 2.616819$ with eight bifurcations is reported.

Furthermore, the dependence $w_{\max}(P_x)$ for the system eigenfrequency $\omega_0 = \omega_p = 3$ is illustrated and its changes *versus* sign of maximal Lyapunov exponent, as well as $w(t)$, $w(\dot{w})$ for periodic and chaotic vibrations, are analyzed. Besides, in Figure 4 the scale characterizing the type of vibrations and deflection changes of half of the plate surface $w(0 \le x \le 1; 50 \le t \le 60)$ for periodic and chaotic dynamics are shown. All of them supplement each other creating a real picture of plate vibrations. The beating regime is observed during transition of the Lyapunov exponent from negative values to zero, which is exhibited by the dependence $w_{\max}(P_x)$. A positive value of the Lyapunov exponent corresponds to chaotic vibrations.

A route to chaos is strictly associated with the Feigenbaum scenario.

In order to trace the complex dynamics, Poincaré sections are introduced for $\omega_p = \omega_0$, $P_x \in [2.7; 3.3]$ with the step 0.01 of P_0 (Figure 5).

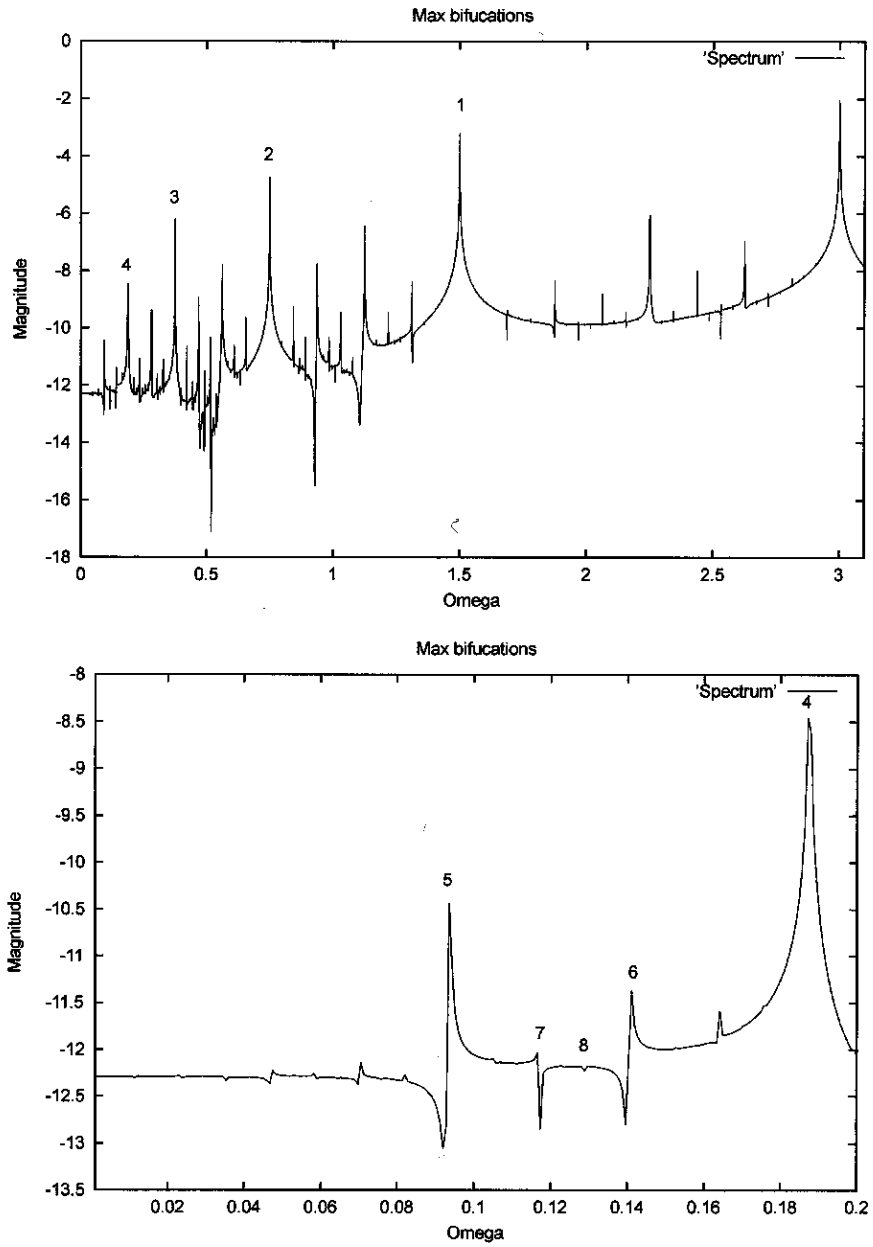

Figure 3. Frequency spectrum with marked eight bifurcations.

For the certain values of P_0 phase portraits and corresponding Poincaré maps are attached (Figure 6). The described observations are additionally supplemented by the signals $w(\dot{w})$, $w(t)$ and frequency power spectra for the characteristic values of $P_0 = 2.61; 2.7; 7$ (Figure 7).

Chaotic vibrations for the considered values (P_0, ω_0) begin from period-doubling bifurcation (this is marked by yellow color). The series of those bifurcations are easily traced in the power spectrum (Figure 2). Eight bifurcations are numerically detected. The process of transition to chaos is characterized by a broad band noise occurring in the spectrum support.

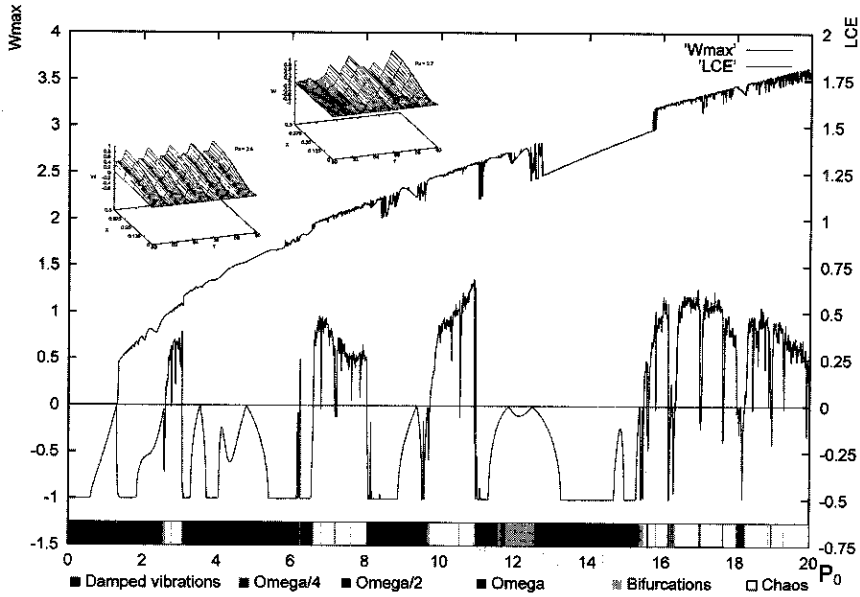

Figure 4. Lyapunov charcateristic exponent and maximal deflection $w_{\max}$ *versus* P_0 and the plate surface shapes.

The peaks corresponding to the fundamental frequencies and their harmonics remain clearly distinguished.

The observed series of period-doubling bifurcations indicates an occurrence in the system of an infinite series of period-doubling bifurcations leading to chaotic vibrations, as well as the self-similarity properties yielded by the 'theory of universality' [19].

The sequence of period-doubling bifurcations approaches the strange chaotic attractor.

After the Andronov–Hopf bifurcation, a stable limit cycle is born and the previously stable equilibrium (singular point) becomes unstable of the saddle-focus type with one-dimensional stable W^s and two-dimensional unstable W^u manifolds. First, the unstable manifold W^u of the equilibrium is the limit cycle. Then the two smallest multipliers of the limiting cycle become complex conjugates. The manifold W^u starts to wind up on the limit cycle and a configuration similar to a funnel appears. All attractors from a certain region are pulled into this funnel. The following situation is possible: W^s and W^u approach each other until the saddle-node homoclinic curve occurs. In this case, quite complex dynamics of the trajectories is expected. Funnel occurrence is expected to yield a chaotic attractor (this attractor is either called the screw type attractor [20, 21], or the spiral attractor).

Motivated by [20, 21] one may wish to distinguish between Smale attractors and attractors occurring in a neighborhood of a saddle-node loop (Shilnikov's attractors). In the case of Smale attractors the time instants corresponding to maximal vibration peaks are distributed in a rather regular way, whereas in the case of Shilnikov's attractors they form a probabilistic sequence.

Besides the previously mentioned Smale and Shilnikov attractors, a Rössler attractor may also appear. The Rössler-type attractor is detected for $\omega_p = 2.25 < \omega_0 = 3$ and is yielded by a series of period-doubling bifurcation. The scenario of its occurrence for the parameter $P_x = 4$; 4.48; 4.5 is reported in Figure 8. The Rössler attractor is present in the last of the shown phase portraits. The associated $w(t)$, $w(\dot{w})$ and power spectrum are also shown in Figure 8.

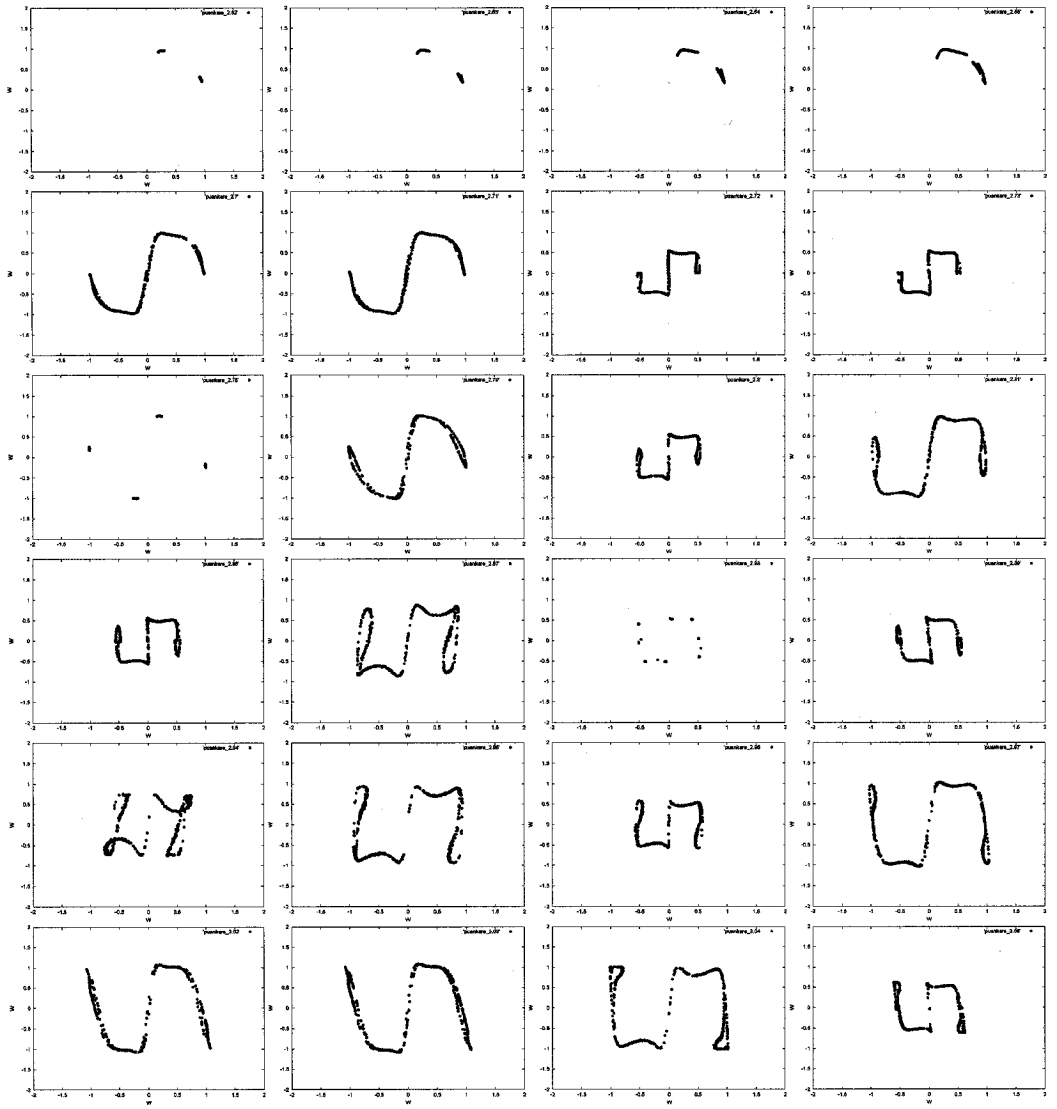

Figure 5. Poincaré sections for different P_0.

7. The Finite Difference Method and Lyapunov Characteristic Exponents

Recall that during the solving of the problem using the finite difference method, the dimension of the system of differential equations is equal to $2n$, where n denotes the number of mesh grids. Since the right-hand side of the investigated system is complicated, it is impossible to find Lyapunov exponents using an analytical approach, as is described in Section 5. Therefore, in the case of the finite difference method the classical approach formulated by Benettin et al. [16, 17] is applied. However, even application of the classical approach requires the use of the Jacobian, which (in our case) is very complicated and is different for different boundary conditions. Therefore, the Jacobian associated with a phase curve is numerically estimated using central difference derivatives with approximation order of $O(h^4)$. Our computations

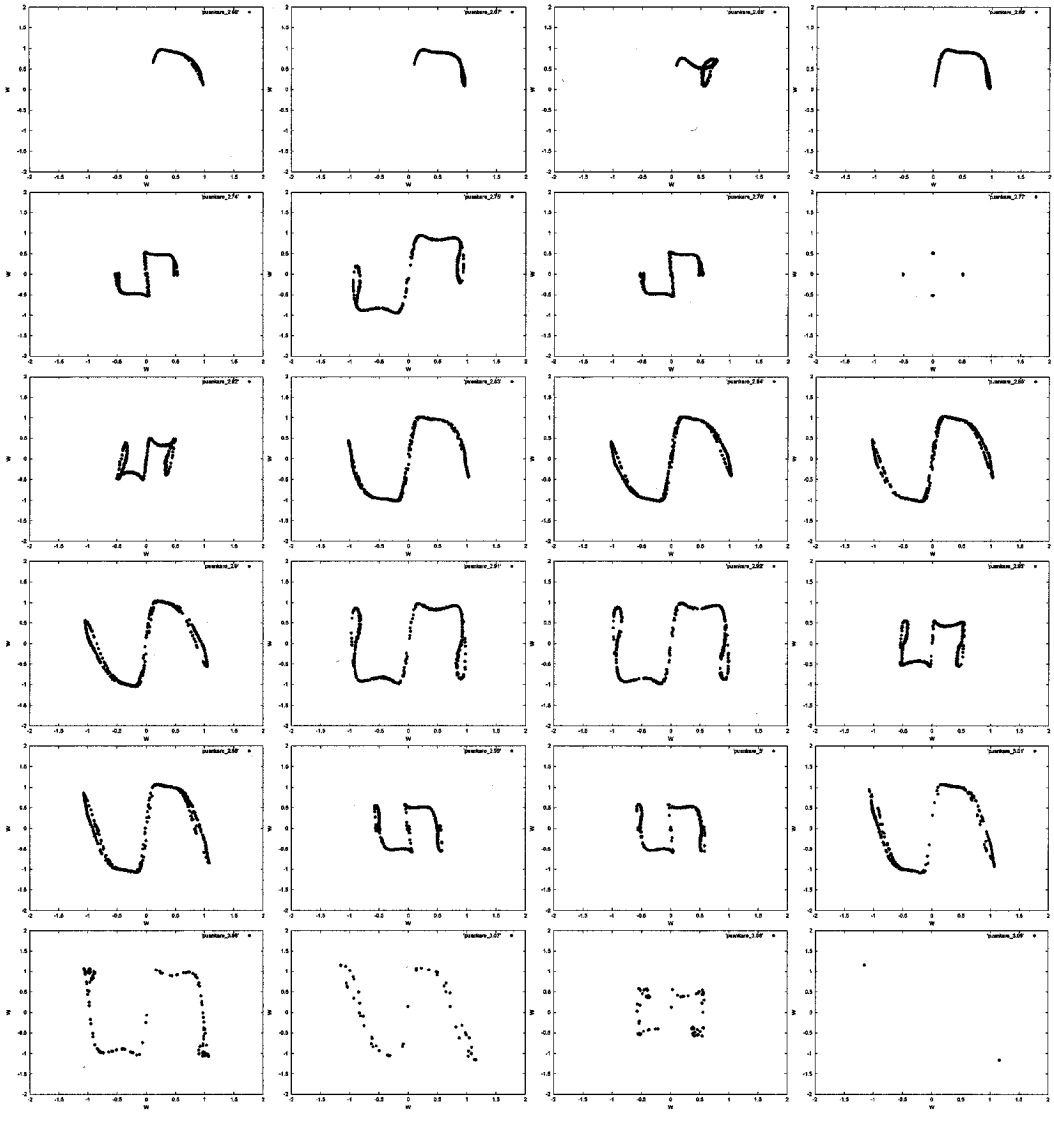

Figure 5. Continued.

only include the largest Lyapunov exponent χ. The dependencies $w_{\max}(P_0)$, $\chi(P_0)$, as well as the scale-characterizing vibrations for boundary conditions (2.3) and initial conditions (2.7) are reported in Figure 9 for $\omega_p = 7$. It is seen that all the obtained characteristics supplement each other and illustrate very well a physical interpretation of the analyzed process.

8. Finite Difference Method (Problem 2)

This problem is similar to problem 1, and it can be also solved using the high-order Bubnov–Galerkin method. However, only the finite difference method is applied, since it is most general and does not require additional mathematical treatment (contrary to the Bubnov–Galerkin method). Note that Equations (2.2), (2.5) and (2.7) are now analyzed.

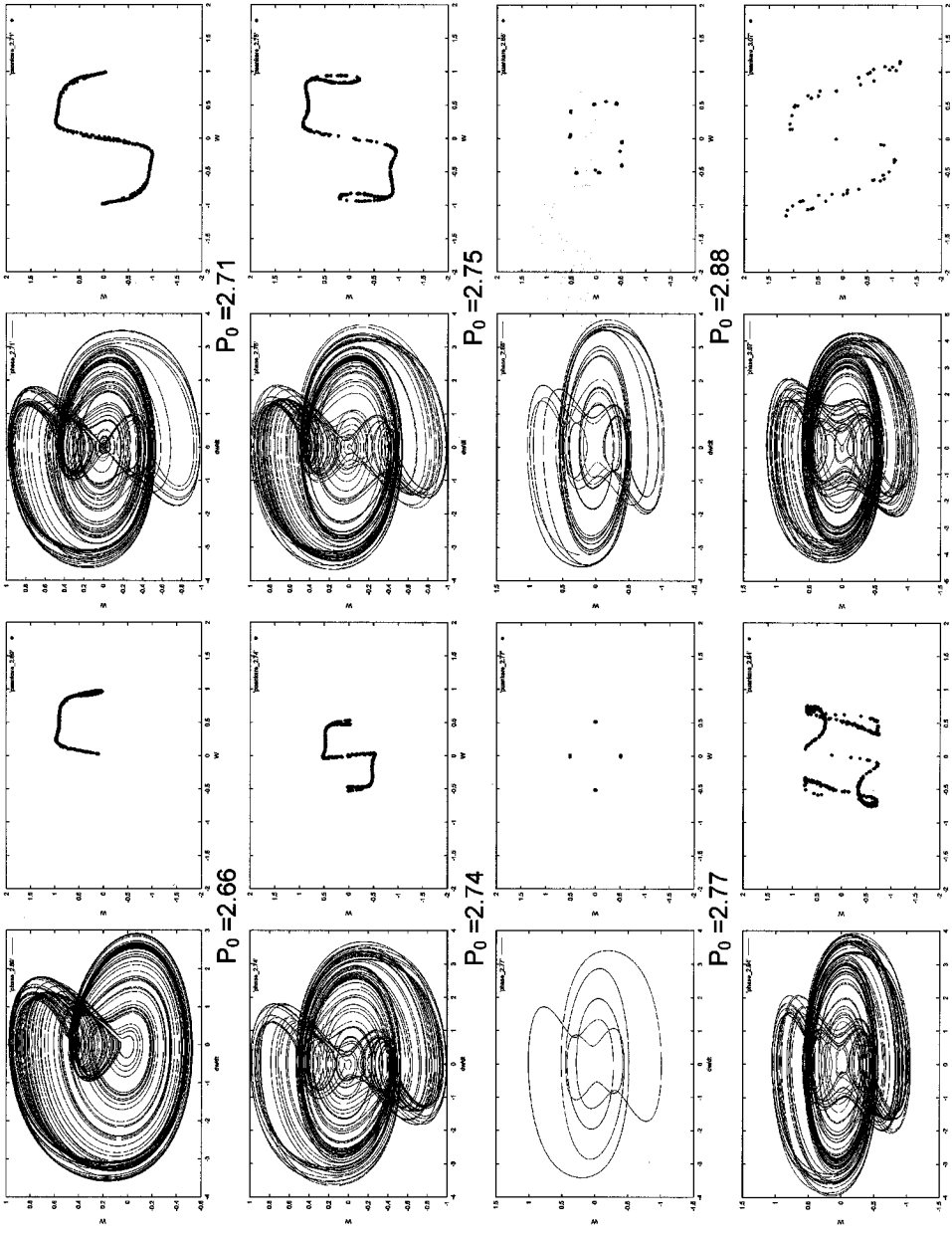

Figure 6. Phase portraits and Poincaré sections for $P_0 = 2.66; 2.71; 2.74; 2.75; 2.77; 2.88; 2.94; 3.07$.

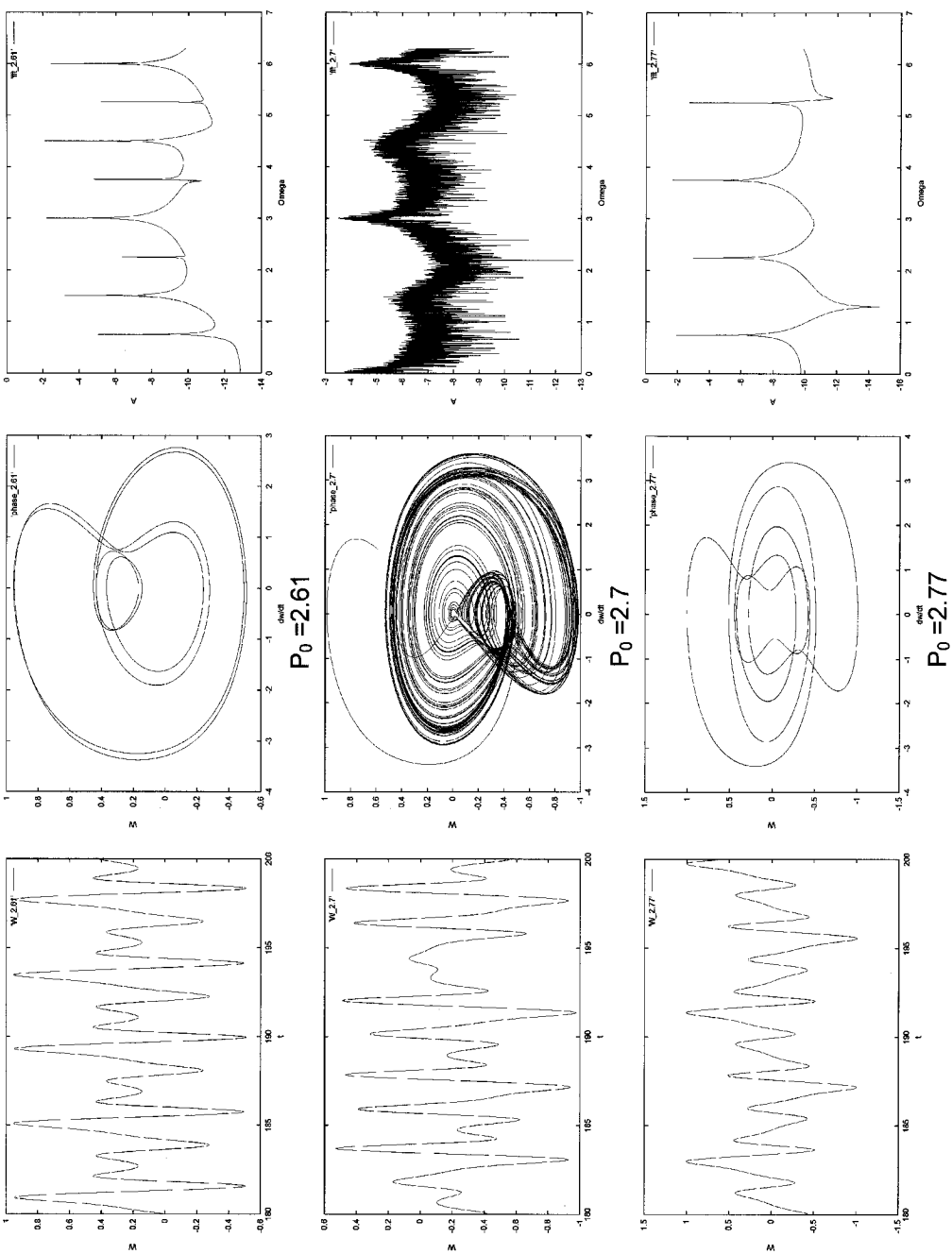

Figure 7. Time histories, phase portraits and power spectra for $P_0 = 2.61; 2.7; 2.77$.

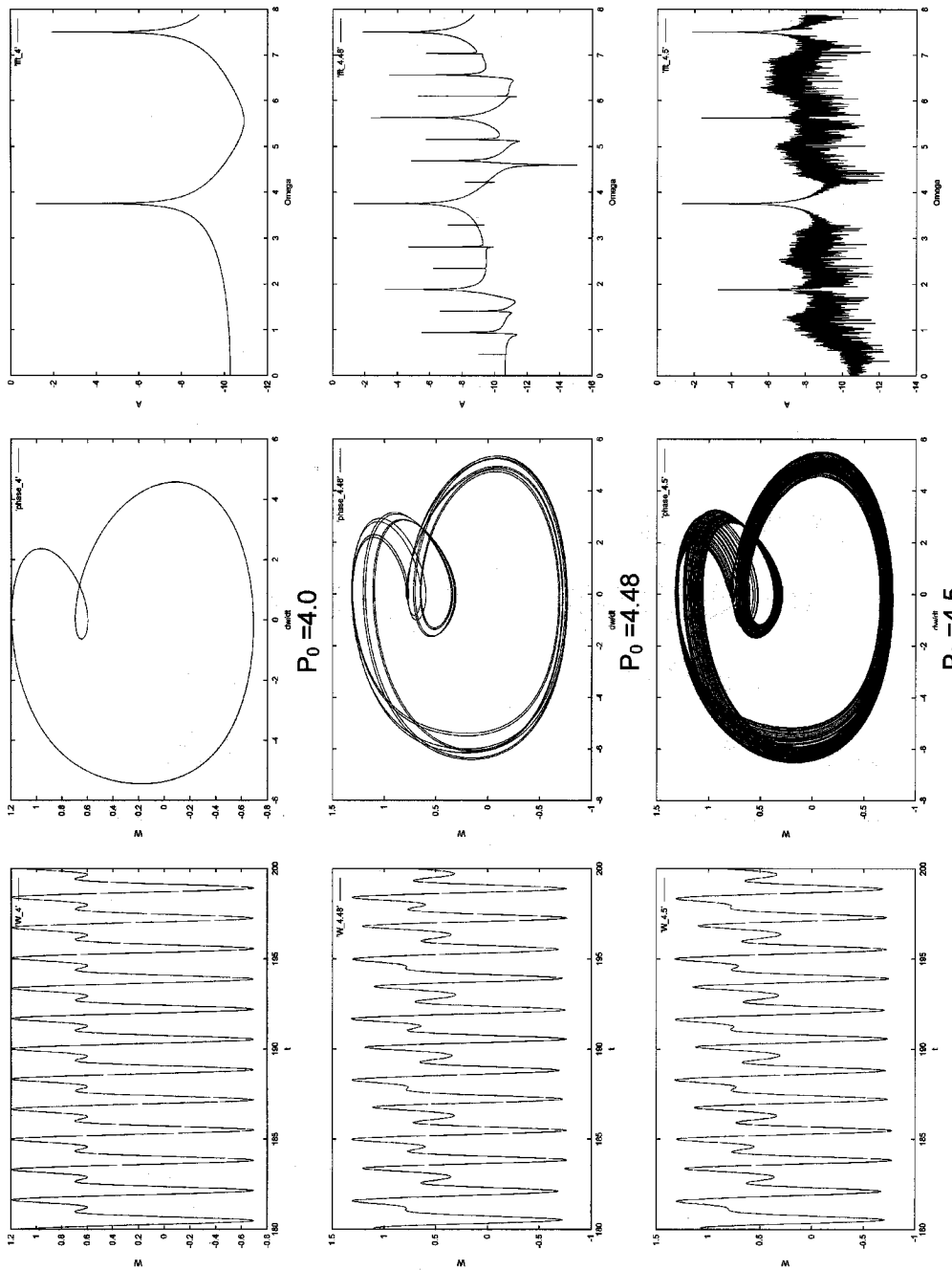

Figure 8. Time histories, phase portraits and power spectra for $P_0 = 4.0; 4.48; 4.5$.

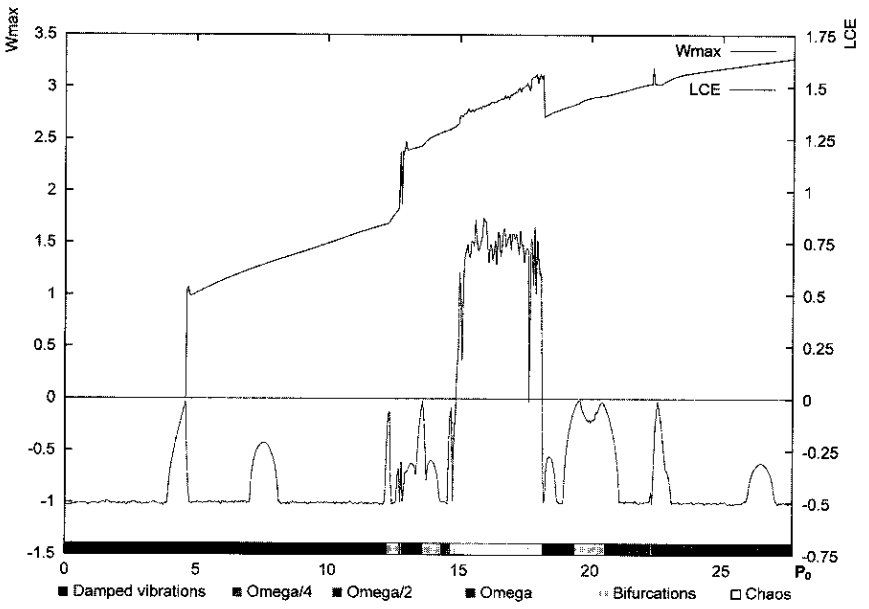

Figure 9. Dependencies $w_{\max}(P_0)$ and the Lyapunov characteristic exponenent $LCE\ (P_0)$.

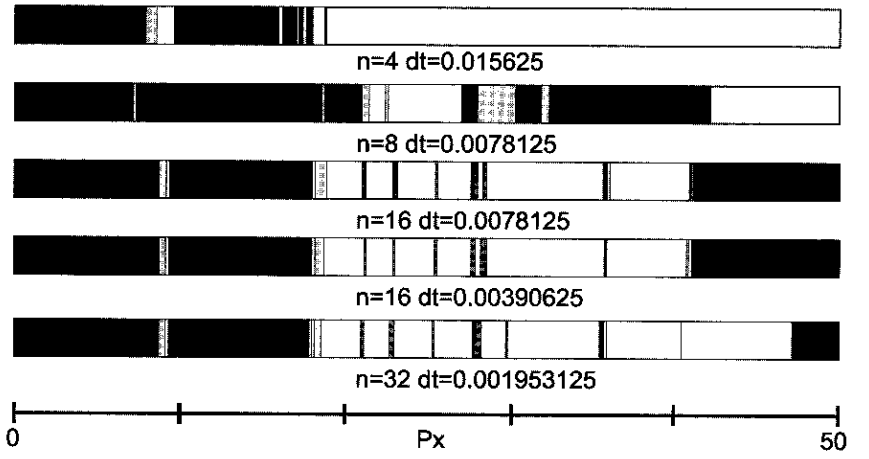

Figure 10. Vibration types for different time and spatial steps.

First, a convergence of the difference scheme is investigated. Applying Runge's rule, the minimal number of grids is estimated, which gives reliable (true) results while constructing a chart. The different vibration types and different grid numbers are shown in Figure 10 ($\omega_p = 5$, $0 < P_0 < 50$). It has been established that the required accuracy is achieved for $n = 16$, $\mathrm{d}t = 2^{-8} = 0.00390625$. Using these parameters, the chart shown in Figure 11 is constructed. The eigenfrequency of the system is equal to $\omega_0 \cong 6.8$ and, therefore, ω_p undergoes variation within the interval (3.0; 10.0). Although, in general, a scenario of the system dynamics is similar to that of problem 1, but there are some peculiarities. In spite of period-doubling bifurcations, the period-tripling bifurcations are also detected. The fundamental characteristic of similar regimes $w(t)$, $w(\dot{w})$ power spectrum and Poincaré sections ($\omega_p = 8.75$, $P_0 = 25.8$) are shown in Figure 12. However, in the case of period-tripling bifurcations, the borders between the different zones were not clearly defined during our

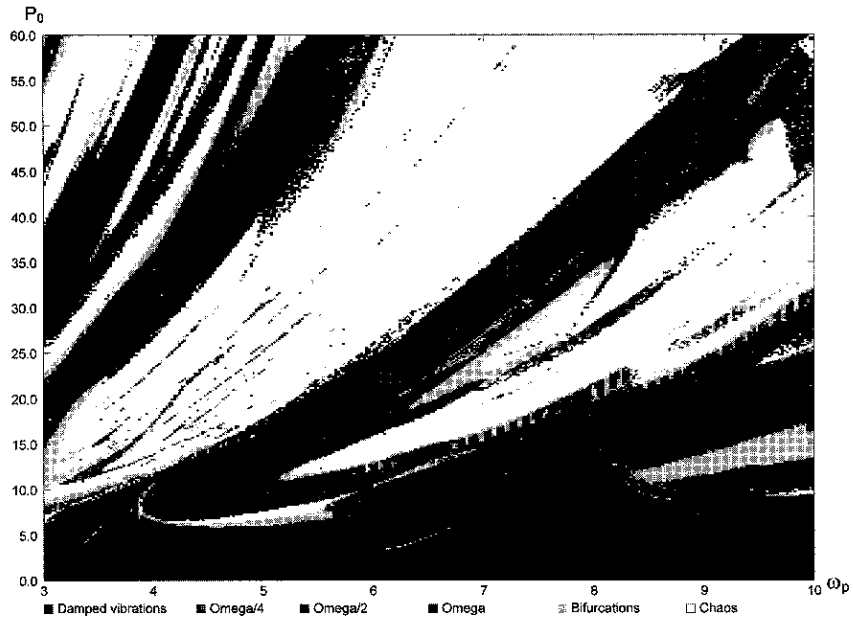

Figure 11. Regular and chaotic dynamics in the plane (P_0, ω_p) (problem 2).

Table 2. Amplitudes of parametric excitation P_0^n and the Feigenbaum constants C_i for the problem 2 (n denotes bifurcation number).

n	1	2	3	4	5	6	7	8
P_0^n	14.68363	14.84414	14.90272	14.91509	14.91784	14.91844	14.91857	14.91860
C_i	2.7395	4.7368	4.5069	4.5705	4.4971	4.6358		

computer experiment, and therefore unfortunately we could not estimate the Feigenbaum-type constants of the investigated process.

In the case of period-doubling bifurcations the Feigenbaum scenario holds. The obtained data are reported in Table 2 ($\omega_p = \omega_0 \approx 6.8$).

9. Credibility of the Obtained Results

In order to be certain of the credibility of the obtained results, a direct comparison between the two computational methods is required. Since the Bubnov–Galerkin and finite difference methods have different structures, a close similarity of the results verifies their credibility. A comparison of application of the two computational methods is carried out in a chaotic zone. Note that an investigation of harmonic oscillations and bifurcation zones using these methods yields the same results. In Figure 13, a second-order bifurcation diagram and the signal $w(0.5, t)$, $0 \leq t \leq 50$, $P_0 = 2.608$ are reported. The dashed curves are obtained using the finite difference method by dividing an interval into 16 parts, whereas the solid curves correspond to the use of Bubnov–Galerkin method and the finite difference method. It is worth noticing that the obtained results differ of less than 0.05%.

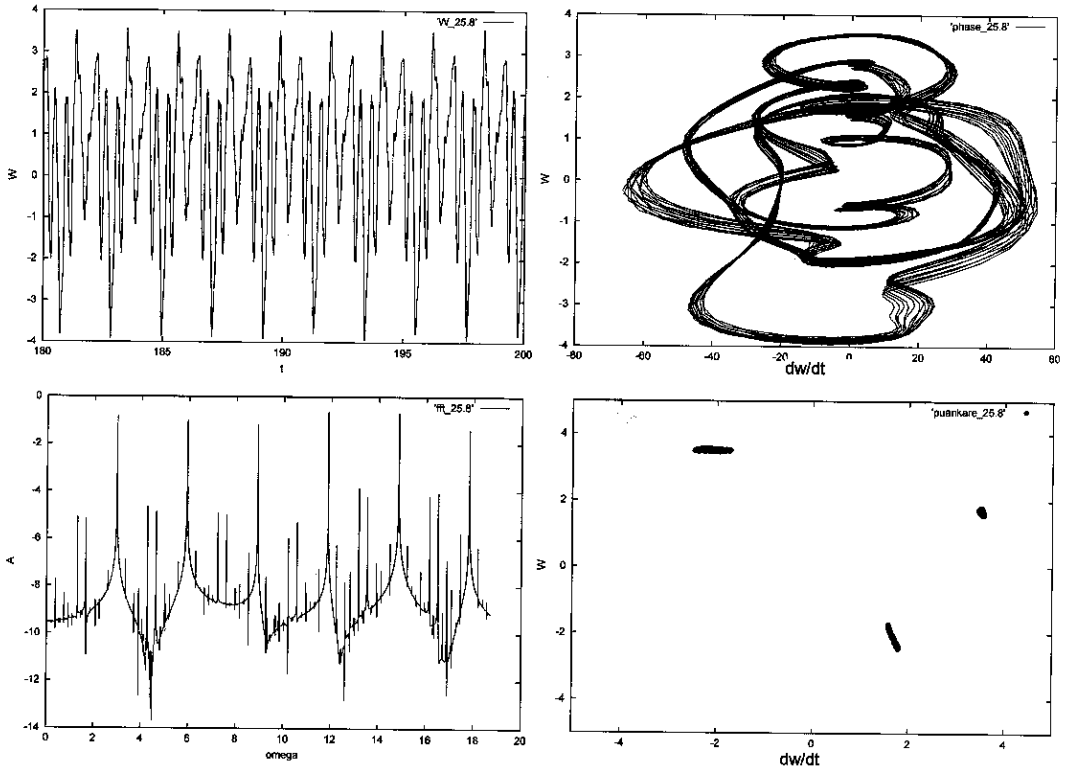

Figure 12. Time history, phase portrait, power spectrum and Poincaré section for $\omega_p = 8.75$ and $P_0 = 25.8$.

Table 3. Amplitudes of parametric excitation P_0^n corresponding to successive bifurcations n obtained using Bubnov–Galerkin (BG) and finite difference (FD) methods.

n	1	2	3	4	5	6	7	8
BG P_0^n	2.5732661	2.6036145	2.6136281	2.6161521	2.6166796	2.6167908	2.6168156	2.6168261
FD P_0^n	2.5744713	2.6046805	2.6146613	2.6171769	2.6176940	2.6178122	2.6178387	2.6178445

In addition, chaotic vibrations are also analyzed for $P_0 = 3.0$, $\omega_p = \omega_0 = 3.0$. The responses obtained using both approaches are reported in Figure 14 for $w(0.5, t)$, $0 \leq t \leq 100$. The same holds for the earlier description for curves. The frequency spectra obtained via Bubnov–Galerkin (in the above) and the finite difference method (in the below) are shown. Although one may observe the differences in the obtained responses, the integral charactrer-istics (power spectra) are fully equivalent. In addition, both obtained (P_0, ω_p) 'charts' via two computational methods overlapped well with each other. The latter case is discussed in more depth in Section 6.

10. Conclusions

Bifurcations and routes to chaos exhibited by a thin plate strip are analyzed. First, fundamental relations, the governing equations, and the attached boundary and initial conditions

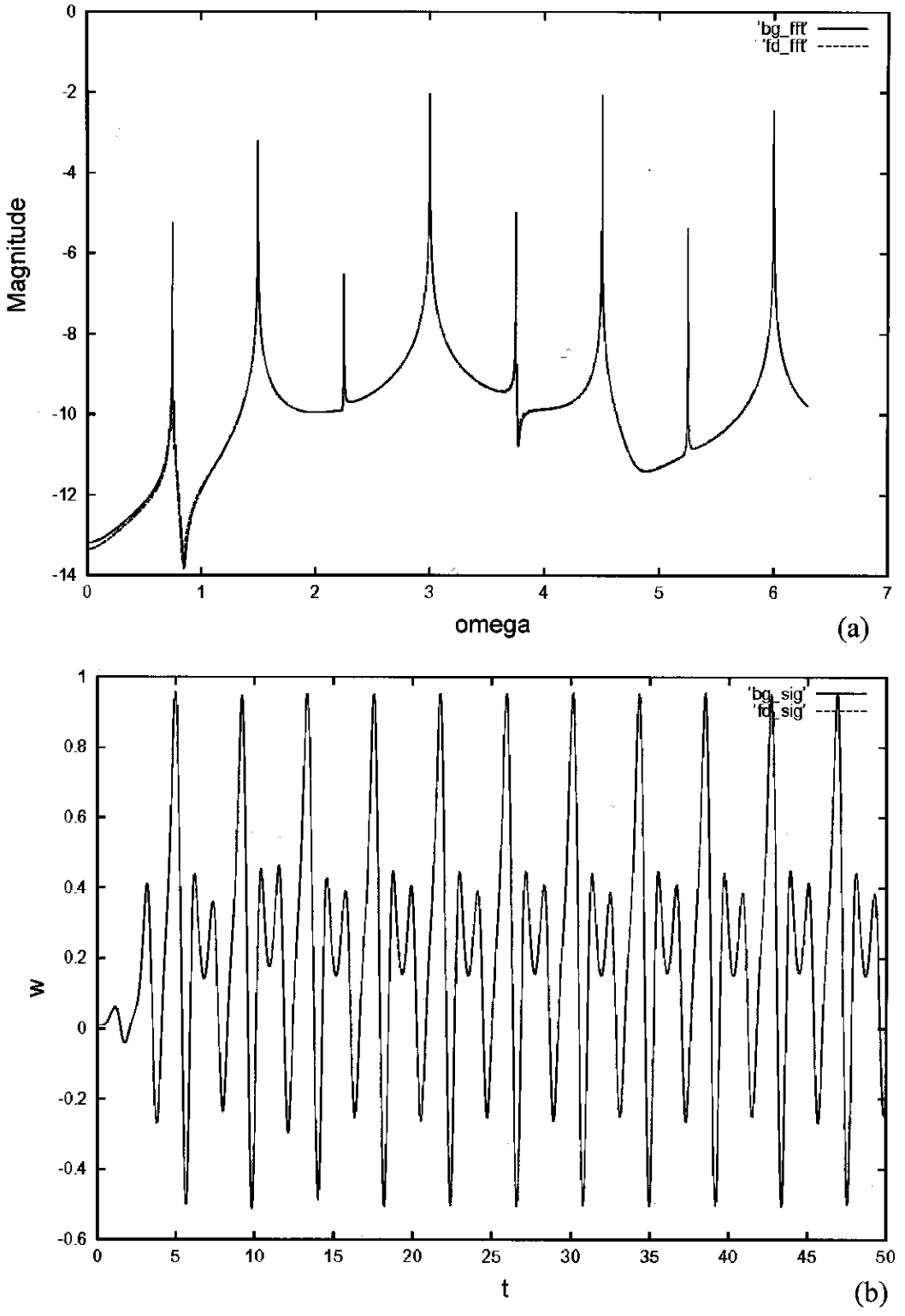

Figure 13. Frequency spectrum (a) and $w(0.5, t)$ obtained using Bubnov–Galerkin (bg) and finite differences (fd) methods.

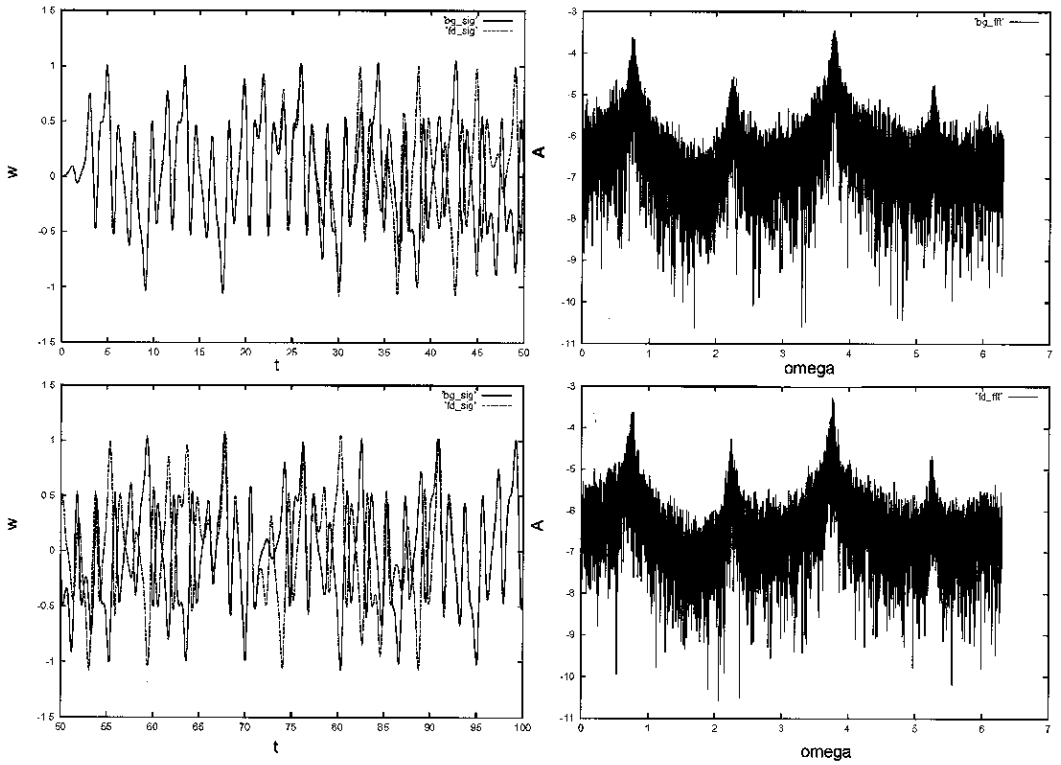

Figure 14. Time series $w(0.5, t)$ of chaotic vibrations and frequency spectrum (bg (fd) correspond to Bubnov–Galerkin (finite difference) method).

are formulated. Then both computational methods used, i.e. the Bubnov–Galerkin method with higher approximations and the finite difference method with an approximation of $O(h^4)$, are described. More attention is paid to the estimation of the characteristics of the Lyapunov exponents using both analytical and numerical methods. Finally, two computational examples are discussed and illustrated. In the first considered problem, the parameter plane (P_0, ω_p) is separated into three qualitatively different parts. Jump-like switching phenomena, series of bifurcations, 'stiff' bifurcations, the Feigebaum-like route to chaos and various types of strange chaotic attractors are reported and discussed.

In the second problem considered, in spite of period-doubling bifurcations similar to that of problem 1, the period-tripling bifurcations are also detected.

The credibility of the obtained results is illustrated and discussed.

References

1. Awrejcewicz, J., Andrianov, I. V., and Manevitch, L. I., *Asymptotic Approach in Nonlinear Dynamics: New Trends and Applications*, Springer, Berlin, 1998.
2. Awrejcewicz, J. and Krysko, V. A., 'Feigenbaum scenario exhibited by thin plate dynamics', *Nonlinear Dynamics* **24**, 2001, 373–398.
3. Awrejcewicz, J., Mrozowski, J., and Potier-Ferry, M., 'Non-linear behaviour of a rectangular plate exposed to airflow', in *Bifurcation and Chaos-Theory and Applications*, J. Awrejcewicz (ed.), Springer, Berlin, 1995, pp. 253–272.

4. Bajaj, A. K. and Johnson, J. M., 'Asymptotic techniques and complex dynamics in weakly nonlinear forced mechanical systems', *International Journal of Mechanics* **25**, 1990, 211–226.
5. Abe, A., Kobayashi, Y., and Yamada, G., 'Two-mode response of simply supported, rectangular laminated plates', *International Journal of Non-Linear Mechanics* **33**(4), 1998, 675–690.
6. Nayfeh, T. A. and Vakakis, A. F., 'Subharmonic traveling waves in a geometrically non-linear circular plate', *International Journal of Non-Linear Mechanics* **29**(2), 1994, 233–245.
7. Wei-Zhang, Zhaomiao, L., and Pei, Y., 'Global dynamics of a parametrically and externally excited thin plate', *Nonlinear Dynamics* **24**, 2001, 245–268.
8. Lasiecka I., 'Finite dimensionality and compactness of attractors for von Kármán equations with nonlinear dissipation', *Nonlinear Differential Equations and Applications* **6**, 1999, 437–472.
9. Krysko, V. A., Awrejcewicz, J., and Bruk, V., 'On the solution of a coupled thermo-mechanical problem for non-homogeneous Timoshenko-type shells', *Journal of Mathematical Analysis and Applications* **273**(2), 2002, 409–416.
10. Krysko, V. A., Awrejcewicz, J., and Bruk, V., 'On existence and uniqueness of solution to coupled thermomechanics problem of non-homogenous isotropic plates', *Journal of Applied Analysis* **8**(1), 2002, 129–139.
11. Awrejcewicz, J. and Krysko, V. A., *Nonclassic Thermoelastic Problems in Nonlinear Dynamics of Shells*, Springer, Berlin, 2002.
12. Awrejcewicz, J., Krysko, V. A., and Krysko, A. V., 'Spatial temporal chaos and solitons exhibited by von Kármán model', *International Journal of Bifurcation and Chaos* **12**(7), 2002, 1465–1513.
13. Volmir, A. S., *Nonlinear Dynamics of Plates and Shells*, Nauka, Moscow, 1972 [in Russian].
14. Fedosev, V. I., 'On the problem of stability of deformable bodies', *Applied Mathematics and Mechanics* **27**(2), 1963, 971–976 [in Russian].
15. Oseledec, V. I., 'A multiplicative ergodic theorem: Liapunov characteristic numbers for dynamical systems', *Transactions of the Moscow Mathematical Society* **19**, 1968, 197–231.
16. Bennetin, G., Casartelli, M., Galgani, L., Giorgilli, A., and Strelcyn, J. M., 'On the reliability of numerical study of stochasticity, I: Existence of time averages', *Il Nuovo Cimento* **44B**(1), 1978, 183–195.
17. Bennetin, G., Casartelli, M., Galgani, L., Giorgilli A., and Strelcyn, J. M., 'On the reliability of numerical studies of stochasticity, II: Identification of time averages', *Il Nuovo Cimento* **50B**, 1979, 211–232.
18. Pesin, Yu. B., 'Characteristic Lyapunov exponents and smooth ergodic theory', *Russian Mathematical Survey* **32**, 1977, 55–114.
19. Bul, B., Sinai, A. G., and Chaikin, K. M., 'Feigenbaum universality and thermodynamic formalism', *Uspekhi Mathematicheskich Nauk* **39**(3), 1984, 3–37 [in Russian].
20. Arneodo, A. and Thual, O., 'Direct numerical simulation of triple convection problem versus normal form prediction', *Physics Letters A* **109**(8), 1985, 367–373.
21. Arneodo, A., Collet, P. M., Spiegel, E. A., and Tresser, C., 'Asymptotic chaos', *Physica D* **14**(3), 1985, 327–347.